

Transient Thermo-Acoustic Responses of Methane/Hydrogen Flames in a Pressurized Annular Combustor

Byeonguk Ahn¹

Department of Energy and Process Engineering,
Norwegian University of Science and
Technology,
Trondheim N-7491, Norway
e-mail: byeonguk.ahn@ntnu.no

Thomas Indlekofer

Department of Energy and Process Engineering,
Norwegian University of Science and
Technology,
Trondheim N-7491, Norway

James Dawson

Department of Energy and Process Engineering,
Norwegian University of Science and
Technology,
Trondheim N-7491, Norway

Nicholas Worth

Department of Energy and Process Engineering,
Norwegian University of Science and
Technology,
Trondheim N-7491, Norway

The present article experimentally investigates the triggering and transient growth of azimuthal instabilities in a pressurized laboratory-scale annular combustor featuring 12 methane/hydrogen flames, as the equivalence ratio is ramped up and down. The ramping rate of equivalence ratio is varied to examine its effect on the transient thermo-acoustic response and the driving mechanisms, highlighting a number of previously unseen features. As the equivalence ratio is dynamically increased, all cases were observed to feature a distinct modal trajectory, during the onset of high-amplitude instabilities. Strongly spinning counterclockwise modes are first excited before a dynamic transition to strongly spinning clockwise modes occurs. Furthermore, the strength of the spinning mode (quantified through the spin ratio or nature angle) was shown to feature a local minima before the spinning mode stabilized in the system, which corresponds to an almost pure spinning state. Hysteresis behavior was observed in both the amplitude and nature of the mode, resulting in different thresholds for the onset and decay of the instability, depending on the time history of the combustor. Increasing the ramping rate was found to reduce the amount of hysteresis in the system. Furthermore, the high amplitude of the instability resulted in significant harmonic components. The behavior of the harmonics generally resembles the fundamental component, albeit with some notable exceptions.

[DOI: 10.1115/1.4052259]

Introduction

Flexible, hydrogen fired gas turbines are predicted to play a vital role in accelerating the energy transition, by providing stability to the grid through dynamic operation, enabling an increasing penetration of intermittent renewable power sources. However, the effect of dynamic operation on azimuthal combustion instabilities has not been investigated under well-defined acoustic boundary conditions before.

Combustion dynamics is a complex phenomenon arising from the coupling between heat release rate and acoustic perturbations, which can occur in a wide variety of combustion systems [1–3]. In rotationally symmetric annular systems, combustion instabilities tend to excite azimuthal modes, as observed in both industrial combustors and aero-engines where the circumference typically has the longest dimension [4–6]. Azimuthal instabilities can produce different oscillatory patterns with the same eigenfrequency, such as standing or spinning modes, or patterns combining features of both, which are described as mixed modes. Time-varying changes in the modal state are one of the important defining features of azimuthal modes, and rapid switching between modes states is commonly referred to as *modal dynamics* [7–12]. Modal dynamics have been found to be largely influenced by symmetry breaking [13–19] and turbulent noise [6,17,20,21].

Many recent studies have been devoted to understanding circumferentially coupled thermo-acoustic oscillations which occur in annular combustors. Azimuthal modes have been reported in industrial [4–6] and lab-scale combustors [10–12,22,23] and in high-fidelity simulations [8,24]. However, most studies have been conducted under atmospheric conditions. A very limited number of investigations have investigated azimuthal instabilities under pressurized (above 189 kPa) operating conditions. Fanaca et al. [25,26] examined dynamic characteristics of premixed flames in

an annular combustor at elevated pressure. They demonstrated through the application of acoustic forcing that an aerodynamic effect causes discrepancies in the flame transfer function behavior between an isolated single flame and flames in the annular combustor. However, self-excited azimuthal instabilities were not reported in this study.

More recently, Mazur et al. [27] investigated self-excited combustion instabilities in a pressurized annular combustion test rig. They observed both longitudinal and azimuthal instabilities under choked conditions. They also reported that the flame stabilization location induces mode transition from longitudinal to azimuthal instabilities at a high equivalence ratio, and that the response is characterized by the existence of multiple higher harmonic contributions. However, azimuthal modes were only observed in a flashback state. This motivated the modification of the bluff bodies in a consecutive study [28], allowing long run times and the study of a wide range of operating conditions. A cut-on amplitude of the instabilities was identified above which harmonic contributions become significant and lead to a strong distortion of the phase space. When the harmonic contributions were significant, interactions between the harmonic components of the pressure amplitudes were shown to follow a quadratic relationship. In terms of the nature of the mode, high-amplitude states featured clockwise spinning modes, while low-amplitude states featured counterclockwise spinning modes with a clear trend toward stronger spinning states with increasing amplitudes.

Most of the aforementioned studies focus on describing combustion instabilities while maintaining constant operating conditions. However, it is also of interest to describe the occurrence and behavior of instabilities in response to time-varying operating conditions. Despite decades of active research, an understanding of the transient dynamics of self-excited instabilities is far from complete, and finding robust precursors that can forewarn of an impending instability remains a crucial issue. The majority of previous studies on transient combustion dynamics have been conducted on single flame configurations [29–34]. It has been found that either inherent noise from turbulence or external noise

¹Corresponding author.

Manuscript received July 15, 2021; final manuscript received August 4, 2021; published online October 18, 2021. Editor: Jerzy T. Sawicki.

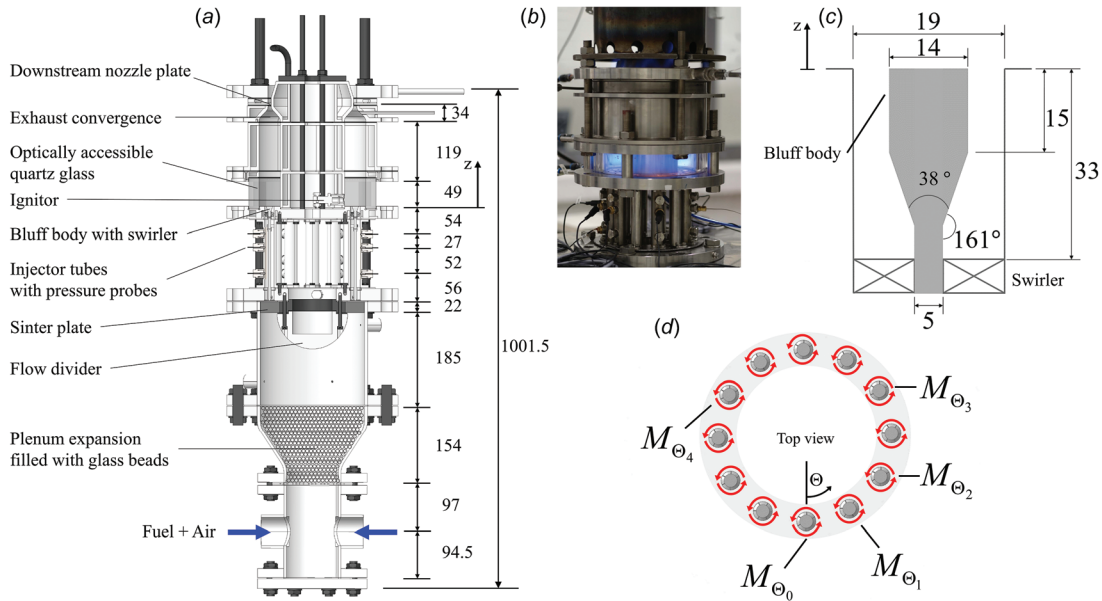


Fig. 1 Experimental setup of a lab-scale pressurized annular combustor with 12 bluff body stabilized flames. (a) Cross-sectional view of the test rig, (b) photograph of IPA combustor during self-excited azimuthal instabilities, (c) lateral view of injector showing the bluff body design and swirler location, and (d) top view of the combustor with positions of microphones installed at $\Theta_{\{k=0,1,2,3,4\}} = 0$ deg, 30 deg, 60 deg, 120 deg, and 240 deg.

induced from an actuator can influence thermo-acoustic dynamics and the onset of subcritical Hopf bifurcations. In an example of an investigation in an annular geometry, Prieur et al. [35] showed that hysteresis controlled the operating limits in the laminar flame matrix burner configurations of the MICCA facility at EM2C. More recently, Indlekofer et al. [36] reported transient acoustic responses in a lab-scale annular combustor under atmospheric conditions subjected to equivalence ratio ramps. It was found that the hysteresis behavior depends on the ramping routes and speeds as well as the power the combustor is operated at. Both positive and negative hysteresis in terms of the amplitude, respectively, decreasing and increasing the stability limits of the combustor, were observed at low power. At increased thermal power, only positive hysteresis was found with decreasing ramp times leading to a larger hysteresis. With increasing amplitudes, the modes were found to transition via standing and mixed modes to strong spinning states at maximum amplitude. However, the transient acoustic responses of azimuthal instabilities under pressurized conditions have not yet been investigated, and therefore the existence of hysteresis effects and the role of higher harmonic components are currently unknown.

In this paper, we investigate the transient acoustic responses during controlled linear upward and downward ramps of the equivalence ratio in a pressurized annular combustor with premixed swirl stabilized methane/hydrogen flames. Several distinct behaviors which depend on the ramping rate are highlighted, such as oscillation amplitude, modal dynamics, and hysteresis. The paper also highlights a number of unexpected and previously unobserved behaviors, such as the overshoot of the nature angle during upwards ramping, which appears to be coupled to the onset of the harmonic response. The insights provided by these experimental results advance our understanding of the transient dynamic nature of azimuthal instabilities under pressurized conditions, which is likely to aid the development of responsive low-emission gas turbines.

Methodology

Experimental Setup and Data Acquisition. Figure 1(a) illustrates a cross section of the lab-scale intermediate pressure

annular (IPA) combustor [27,28], equipped with swirling injectors. The primary components of the test platform include a mixing chamber, a plenum which is partially filled with glass beads, the annular combustion chamber, and a nozzle plate which chokes the flow at the exit.

A premixed $\text{CH}_4\text{-H}_2\text{-air}$ mixture at room temperature (293 K) enters the plenum and flows through a bed of glass beads in the expansion, which is installed to remove large-scale flow structures. The mixture passes through an acoustically reflective 22 mm thick sintered metal plate. The sintered plate has a mean pore size of $183 \mu\text{m}$, porosity 0.12, and $\Delta p \approx 15 \text{ kPa}$ at the flow rate range selected in this study. The flow is then divided into 12 injector tubes which have an inner diameter of $D_{\text{inj}} = 19 \text{ mm}$. Each injector tube has a central rod ($D_r = 5 \text{ mm}$), which expands linearly at an angle of 38 deg (cone-angle) over a streamwise distance of 10 mm. The diameter of the central rod is 14 mm at the bluff body, which was increased from the initial design [27] in order to prevent flashback [28]. Counterclockwise six-vane axial swirlers are mounted 33 mm upstream of the dump plane. The design of the swirlers has been described previously by Worth and Dawson [11].

The water-cooled annular combustion chamber has a length of 168 mm, with an inner and outer diameter of $D_i = 128 \text{ mm}$ and $D_o = 212 \text{ mm}$. The cooling flow was passed through three separate paths, including the inner walls, outer walls, and dump plane of the combustion chamber. The heat transfer over the walls is measured to be $P_{\text{cool-i}} \approx 100 \text{ kW}$, $P_{\text{cool-o}} \approx 50 \text{ kW}$, and $P_{\text{cool-d}} \approx 15 \text{ kW}$. At the exit of the combustion chamber, an area reduction takes place through a symmetric matched fifth-order contraction of length of $L_{\text{CR}} = 34 \text{ mm}$ with a contraction ratio of $\text{CR}_c = 7$. Additionally, a replaceable choking plate is installed with $\text{CR}_p = 5$. This leads to a total contraction ratio $\text{CR}_{\text{tot}} = 35$ at the exit.

Instrumentation and Data Acquisition. Kulite XCE-093 pressure transducers (sensitivity $1.4286 \times 10^{-4} \text{ mV/Pa}$) were used to measure the acoustic fluctuations. To fully characterize the modes and their harmonic components, a total of 12 microphones were installed at five circumferential locations as shown in Fig. 1. At three of these locations, $\Theta_{\{k=1,3,4\}} = 30 \text{ deg}, 120 \text{ deg}, 240 \text{ deg}$,

Table 1 Operating conditions

Case	P_H	P_V	\dot{m}_{air} (g s ⁻¹)	ϕ	t_R (s)
1					10
2	0.10	0.25	95.6	0.7–1.0	5
3					2

microphones were installed at three different axial locations of $z = -54, -81, -133$ mm upstream of the bluff body ($z = 0$ mm). At $\Theta_{\{k=0\}} = 0$ deg, two microphones were installed at $z = -81, -133$ mm, and at $\Theta_{\{k=2\}} = 60$ deg one microphone was installed at $z = -81$ mm. The pressure signals were conditioned by an amplifier (Fylde FE-579-TA) and acquired at a sampling rate of 51.2 kHz. Signals were digitized by a 16-bit data acquisition system (NI 9174).

In order to characterize transient behavior, a number of quantities were locally averaged. The sliding average mean chamber pressure, \bar{p} , was calculated by taking the average of the five circumferential measurements at the location $z = -81$ mm. Then, a sliding average was calculated using a kernel width of 0.1 s.

A summary of the operating conditions is listed in Table 1. The chosen fuel was a methane hydrogen blend. The volume fraction of hydrogen, $P_V = \dot{V}_{\text{H}_2} / (\dot{V}_{\text{CH}_4} + \dot{V}_{\text{H}_2})$, was set to 0.25. This corresponds to a thermal power ratio of hydrogen, $P_H = P_{\text{H}_2} / (P_{\text{CH}_4} + P_{\text{H}_2}) = 0.1$. The air mass flow rate was maintained at 95.6 g s⁻¹. The mass flow rates of the premixed fuel–air mixture were controlled by Alicat mass flow controllers (MFCs) which have an accuracy of 0.8% of the reading plus 0.2% of the full scale. The full scale of MFCs was 5000 SLPM for air and 1000 SLPM for fuel.

The equivalence ratio was varied linearly between $\phi = 0.7$ and 1.0 by controlled ramps. As described in Ref. [28], $\phi = 0.7$ corresponds to a thermo-acoustically stable state at constant operating conditions, and $\phi = 1.0$ corresponds to a strong azimuthal instability. The time duration of the ramps, t_R , was varied between experiments, with values of 10, 5, and 2 s for both upwards and downwards ramps. The combustor was cooled down after each test, and then reignited and preheated before each new test. Despite combustor operation prior to the start of the ramp, the results are described with reference to the starting time of each upward ramp, which corresponds to $t = 0$ s. A total of three repeats was performed for each operating condition. Finally, it is important to note that there is an estimated time delay of ≈ 0.30 s between setting an operating condition at the MFCs and the mixture composition reaching the combustion chamber. This estimated time delay has been included in the time-dependent variation of the equivalence ratio in all subsequent figures. It should also be noted that the uncertainty in the time delay estimate is 0.01 s, which corresponds to a maximum uncertainty of 0.01 for the equivalence ratio in the range $\phi = 0.7 - 1.0$, and of 0.04 m s⁻¹ for the bulk velocity.

Mode Characterization. To characterize the fundamental ($n = 1$) and harmonic contributions ($n = 2 - 5$) of the azimuthal modes, the pressure time series is bandpass-filtered with a bandwidth of 50 Hz around the frequency of interest. Following the approach of Ghirardo and Juniper [37], the acoustic pressure oscillations in an annulus can be represented by

$$p(\Theta, t) = A \cos(n(\Theta - \theta)) \cos(\chi) \cos(\omega t + \phi) + A \sin(n(\Theta - \theta)) \sin(\chi) \sin(\omega t + \phi) \quad (1)$$

where Θ is the azimuthal coordinate, n is the order of the mode, and A , χ , θ , and ϕ are the four slow-flow variables describing the mode. A is the amplitude of the mode, and θ is the position of the antinodal line which we bound between 0 and π in our investigation. The nature of the azimuthal eigenmode is indicated by χ , and

it describes a standing mode if $\chi = 0$, a pure clockwise or counter-clockwise spinning mode if $\chi = -\pi/4, +\pi/4$ or a mix of both for $0 < |\chi| < \pi/4$. The notation of the spin direction orientation is based on the top view of the combustor which corresponds to the coordinate system shown in Fig. 1(d). The sliding average nature angle, $\bar{\chi}$, was calculated using a kernel width of 0.1 s.

The pressure amplitudes of the modes are evaluated at $z = -81$ mm, as the large number of sensors at this axial location allows the identification of azimuthal modes up to the fifth-order using Eq. (1). While the nature of the azimuthal modes does not depend on the axial measurement location, the amplitude does have some dependence due to the acoustic mode shape within the inlet ducts.

Results

Stable to Strong Azimuthal Instabilities. Figures 2 and 3 show time series analysis during both the upward and downward ramps for time durations of $t_R = 10$ and 2 s. The figures present transient time series for a range of metrics describing the time-varying mode state. The left-hand side column shows the complete time series of the experiment, and the two columns on the right side show zoomed-in views of the metrics observed during onset and decay of the high-amplitude instability.

The $t_R = 10$ s case shown in Fig. 2 will be described initially. In the upper row, the red line shows the time-varying equivalence ratio, which is $\phi = 0.7$ until the ramp is initiated at $t = 0$ s. Then, ϕ is increased linearly until it reaches $\phi = 1.0$ at $t = 10$ s. The pressure oscillation amplitude is also shown in the top row. As the equivalence ratio reaches a critical value of $\phi \approx 0.8$, the pressure oscillation amplitude increases dramatically, corresponding to the growth of an azimuthal instability to its limit cycle amplitude. This growth can be seen more clearly on the top row of center column. The downward ramp is then initiated at $t \approx 12$ s, and the equivalence ratio is shown to decrease linearly until it returns to $\phi = 0.7$. Again, at a critical value of ϕ , the pressure oscillation amplitude decreases dramatically, as the combustor returns to a stable state. The decay of the mode is shown on the right-hand side. It is worth noting that the return to a stable state occurs at $\phi \approx 0.72$, which is significantly lower than the onset condition. The difference in operating conditions for the onset and decay of the instability indicates the presence of hysteresis in the system, which has also been observed previously in other annular setups at atmospheric pressure [35,36], and will be discussed later in the Hysteresis section.

It is interesting to note that after the onset, the pressure oscillation amplitude remains relatively stable, with only minor variations in amplitude. The normalized pressure amplitude is around 2% of the mean chamber pressure, and the normalized velocity amplitude at the dump plane is around 20% of the bulk velocity. The second row shows the mean chamber pressure, which closely mimics the variation in ϕ , thereby increasing as the combustor temperature rises with flame temperature at high equivalence ratios. It is worth noting that a fully reflecting boundary condition ($\bar{p} \geq 189$ kPa) is maintained for all cases. The variation in chamber temperature also results in the variation of instability frequency, which can be seen in the spectrogram on the bottom row.

In order to characterize the modal dynamics more accurately, the normalized amplitudes of the fundamental and harmonic components are plotted in the third row, colored by mode order n . As seen in previous studies [27,28] of self-excited azimuthal modes in a pressurized annular combustor, the modes are characterized by large oscillation amplitudes ($A/\bar{p} \approx 2\%$), and the presence of significant amplitude harmonics. The excitation of high-amplitude harmonics is likely related to the use of the acoustically closed nozzle, which results in less damping of higher-order modes in comparison with the open end of previous atmospheric studies [11]. The amplitudes of the fundamental and harmonic components show time-varying behavior, which is classified into

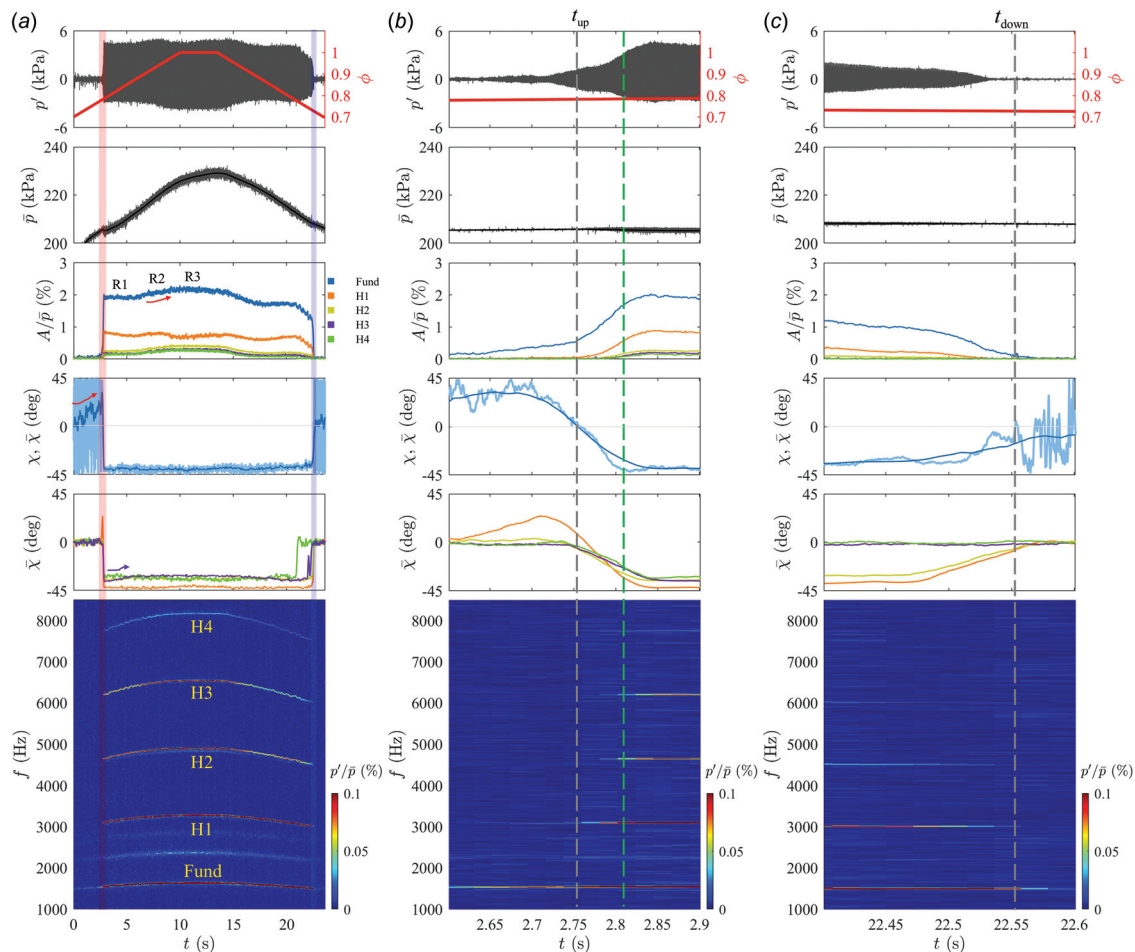


Fig. 2 Time series analysis for $t_R = 10$ s. From top to bottom: Transient time trace of amplitude of pressure oscillations at $\Theta = 30$ deg and $z = -81$ mm, overall equivalence ratio, chamber pressure averaged by using five pressure sensors at $\Theta_{(k=0,1,2,3,4)} = 0$ deg, 30 deg, 60 deg, 120 deg, and 240 deg and $z = -81$ mm, normalized amplitude of fundamental and higher harmonic components with averaged chamber pressure, local and sliding average values of nature angle of the fundamental mode, sliding average values of higher harmonics, and spectrogram of chamber pressure at $\Theta = 30$ deg and $z = -81$ mm with a cutoff of 0.1% for clear visibility. From left to right: (a) Overall time span, stability border during (b) upward (red shaded region) and (c) downward (blue shaded region) ramp. Test conditions: $P_H = 0.1$ and $\phi = 0.7-1.0$.

different regions. Immediately after the onset of the instability, the region R1 has an approximately constant normalized amplitude from $t = 3$ s to $t = 6$ s, despite the increasing pressure and equivalence ratio. The second region R2 from $t = 6$ s to $t = 10$ s sees the normalized amplitude of the fundamental and harmonic components increase significantly. A notable exception however is the first harmonic, which remains relatively constant and even decreases slightly as the other components peak. In the third region R3, the amplitude of the fundamental and all harmonic components remains constant again, from $t = 10$ s to $t = 14$ s, again despite the varying pressure and equivalence ratio. Corresponding amplitude varying and plateau regions also are seen to occur during the downward ramp.

The relatively modest variation in instability amplitudes with operating condition is somewhat consistent with previous measurements under stable operating states, which indicated that the amplitude does not vary as a strong function of equivalence ratio [28] as soon as the combustor becomes strongly unstable. However, comparing the time-dependent amplitude with the frequencies shown in the spectrogram permits similar plateau regions and slopes to be identified. Therefore, it is conjectured that increasing the equivalence ratio modulates the frequency, resulting in minor changes to the instability amplitude.

The fourth and fifth rows describe the nature angle, χ , of the fundamental and harmonic components, which are color coded by

mode order, n . Before the onset of the high-amplitude instability, there are large variations in the nature angle which are dominated by noise. Just before the onset of high-amplitude instabilities however, the fundamental and first harmonic take distinct positive nature angles, corresponding to a counterclockwise (CCW) spinning mode at a low amplitude. As the amplitude of the instability increases, the fundamental and first harmonic components switch to negative nature angles close to the $\chi = -45$ deg limit, which corresponds to a strong clockwise (CW) spinning mode. During the ramp, several parameters may affect the change in the system response. Among these is the flow rate, which may affect the bulk swirl around the annulus. The bulk swirl has been previously linked to a switch of the spinning direction of azimuthal modes in an electroacoustic analogue of an annular combustor [38]. A possible mechanism for such a dependence has been recently identified as the sensitivity of the flame response to the nature angle of the acoustic mode [39,40]. The recent modeling study by Ghirardo et al. [41] demonstrated that the nature angle dependency of the flame gain can give rise to a distinct modal preference for one spin direction over another. In this study, if the bulk swirl changes with the transient change in operating condition, the nature angle dependence of the gain may also change, and with it the preferred mode of excitation. We hypothesize that this may play a major role in the switching of the nature angle observed in our experiments. This mode switch can be clearly observed in the central

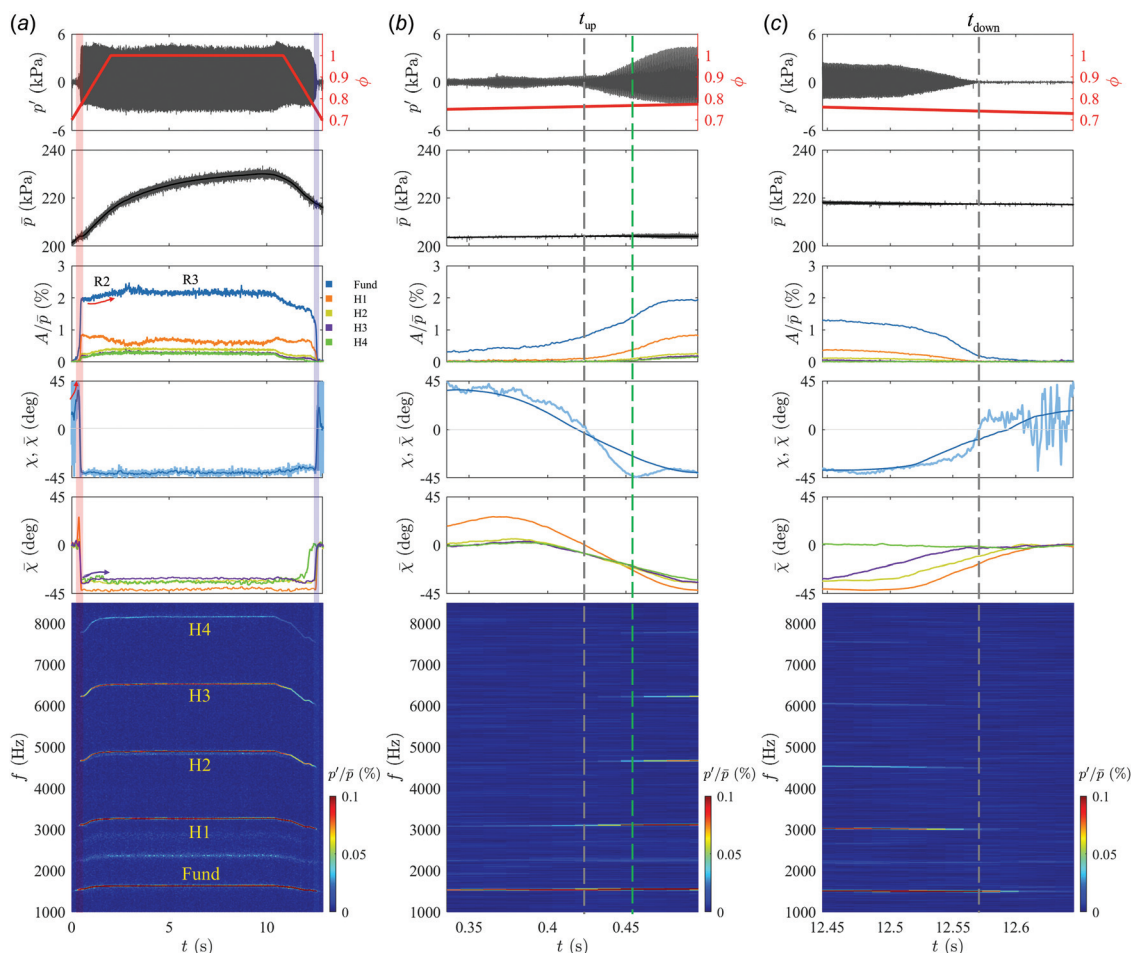


Fig. 3 Time series analysis for $t_R = 2$ s. From top to bottom: Transient time trace of amplitude of pressure oscillations at $\Theta = 30$ deg and $z = -81$ mm, overall equivalence ratio, chamber pressure averaged by using five pressure sensors at $\Theta_{(k=0.1,2,3,4)} = 0$ deg, 30 deg, 60 deg, 120 deg, and 240 deg and $z = -81$ mm, normalized amplitude of fundamental and higher harmonic components with averaged chamber pressure, local and sliding average values of nature angle of the fundamental mode, sliding average values of higher harmonics, and spectrogram of chamber pressure at $\Theta = 30$ deg and $z = -81$ mm with a cutoff of 0.1% for clear visibility. From left to right: (a) Overall time span, stability border during (b) upward (red shaded region) and (c) downward (blue shaded region) ramp. Test conditions: $P_H = 0.1$ and $\phi = 0.7-1.0$.

column. Furthermore, the fact that there is a strong change in nature angle preceding the onset of the instability highlights a potentially useful mechanism for detecting the onset of limit cycle behavior. However, further studies are required to better understand the generality of this observation.

It is interesting to note that during the sudden mode shift to a clockwise spinning mode, the nature angle of the fundamental component exhibits a local minima at -45 deg, before it stabilizes at around -42 deg. A vertical dashed green line is used to highlight the time $t \approx 2.82$ s at which this local minima occurs. This apparent overshoot behavior of the fundamental component nature angle therefore produces instantaneously an almost pure spinning mode; an event that has not been observed in a repeatable manner in previous experiments. It can also be observed that this time instance corresponds to the growth in amplitude of the harmonic components. This can be observed in the amplitude time series on the third row, and also in the spectrogram on the bottom row. It should also be noted that this local nature angle minima occurs in advance of the maximum mode amplitude.

While repeatable overshoot behavior resulting in an extreme spinning state has not been previously observed, preferential modal trajectories have been seen in previous studies. For example, the study by Worth and Dawson [42] shows a number of characteristic patterns occurring during mode switching between

spinning and standing states, including quasi-periodic mode switching trajectories between different states during steady operation. We hypothesize that these modal trajectories may be able to be captured by low-order modeling approaches, which have been used recently to capture mode preferences [41] and mode switching behaviors [19]. The present observations may be useful for evaluating the performance of numerical models due to both the high level of repeatability and the well-controlled acoustic boundary conditions.

Similar to previous findings [28], the closed acoustic boundary condition results in the generation of very high-magnitude azimuthal instabilities. The generation of high-magnitude instabilities will reduce the ability of turbulent noise to push the mode into another state [19], which is likely the reason that the mode never switches out of the CW spinning state when it is reached. A notable difference compared to the investigation at atmospheric pressure [36] is the rapid amplitude growth observed in this study. In Ref. [36], the amplitude increased continuously over large parts of the ramping time with several intermediate jumps depending on the operating condition, while in this study one rapid amplitude growth over a very short time span ($\Delta t \approx 0.05 - 0.1$ s depending on the ramping speed) was observed.

Figure 3 shows the same range of metrics for the shortest ramp time cases, $t_R = 2$ s. Despite the significantly faster ramping rate,

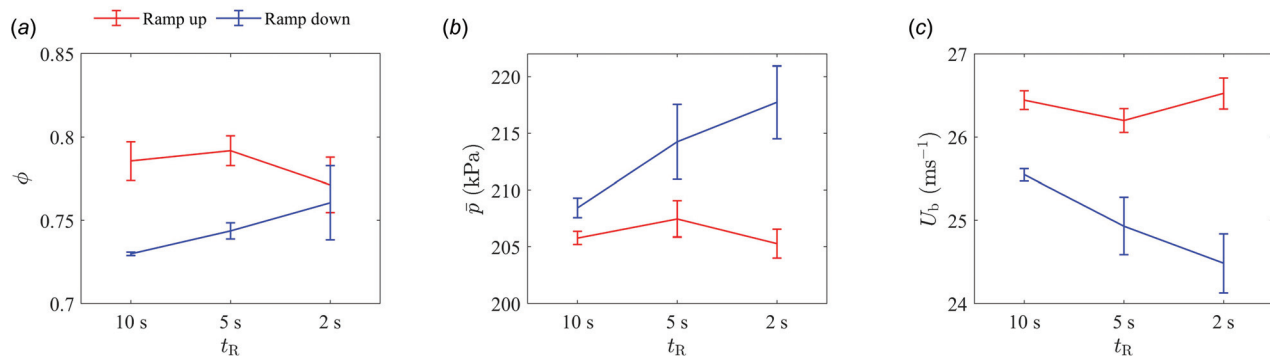


Fig. 4 Averaged equivalence ratio, mean chamber pressure, and bulk velocity during mode transition for both ramping directions. Time-averaged values during mode transitions between stable and unstable state were used to calculate mean values and standard deviation for each repeat case. The figure shows (a) equivalence ratio, (b) mean chamber pressure, and (c) bulk velocity.

in general, many of the same features can be identified, including the instability onset and decay behavior, and the preferential mode switching at onset from CW to CCW with an overshoot to extreme spinning states. However, a number of differences can also be observed.

The equivalence ratio at which the onset and decay of instability occur is slightly lower and higher than the $t_R = 10$ s case, respectively. The combustor pressure response is also observed to react slower to the change in equivalence ratio, which may be related to thermal inertia in the rig. However, the gas temperature responds rapidly to the changing flame temperature, and therefore the frequency changes observed on the spectrogram feature large plateau regions which are similar in extent to the variation of equivalence ratio. Therefore, the amplitude dependence of the fundamental and harmonic components is observed to not feature an initial plateau (the region previously identified as R1), but starts with an initial growth, which is then followed by a long plateau (with these regions marked as R2 and R3, respectively), which again mimic the variations in instability frequency, rather than the chamber pressure. It is noteworthy also that the time duration of the R2 regions is much shorter than the $t_R = 10$ s case, due to the increased ramping rate.

To further quantify differences in the timing of the onset and decay of the instability, Fig. 4 shows the average equivalence ratios, mean chamber pressure, and bulk flow velocities at which the mode transitions occur for both upward and downward ramps. For each ramp, the metrics are evaluated during the switch of the nature angle (specifically when it goes through $\chi = 0$, see gray dashed lines in Figs. 2 and 3) which marks the onset/decay of the strong azimuthal instability. Then, the average values and standard deviations were calculated based on repeat measurements. It should be noted that the bar markers are used to represent the standard deviation of the various quantities, giving therefore an estimate of the variability between independent experiments, rather than an estimate of uncertainty in the measurements themselves.

For the upward ramp, the mode transition occurs at an equivalence ratio of around $\phi = 0.78$ – 0.8 for all cases. For the downward ramp, the transition occurs at the equivalence ratio of around $\phi = 0.72$ – 0.76 with a weak trend of decreasing equivalence ratio at which the transition occurs with decreasing ramp time. Therefore, decreasing the ramping time appears to reduce hysteresis, which is not consistent with previous work [36].

The mean chamber pressure at the onset of the azimuthal instability ranges from 204 to 207 kPa, showing no significant variation with ramping rates. However, the mean chamber pressure during the decay of the instability increases as ramping time decreases. This may be connected with the relatively slow chamber pressure response observed previously. This also may explain why the onset occurs at higher equivalence ratios, but lower chamber

pressures, and vice versa for the decay of the instability. The variation in the bulk flow velocity is directly coupled to the chamber pressure and therefore presents inverse behavior. However, it is worth highlighting that the bulk flow velocity does not change significantly for this range of chamber pressures at onset, and therefore the changes in response observed are more likely connected to the frequency variation of the instability described previously. Finally, in general, the standard deviation of equivalence ratio, mean pressure, and velocity decrease with increasing ramp time, meaning the longer ramp time transition points are more repeatable. This may be expected in a process heavily influenced by the presence of noise, as the critical conditions suitable for the growth or damping of the instabilities are reached more gradually, resulting in transitions which are less dependent on the stochastic fluctuations.

Hysteresis Behavior. While evidence of hysteresis in the instability onset and decay was identified in the Stable to Strong Azimuthal Instabilities section, we now present a more direct analysis of this behavior in terms of the instability amplitude and nature angles during both the upward and downward ramps.

Figure 5 shows the dependence of the normalized fundamental and harmonic component amplitudes on equivalence ratio during upward and downward ramps. Points are binned according to equivalence ratio (with a bin size of 0.005), and for each equivalence ratio bin the mean and standard deviation are plotted. The solid lines show the average behavior, and the standard deviation is presented by shaded regions. It is important to note that representing the data in this manner does not allow the time history to be shown directly. However, due to the large change in amplitude and nature angle which occurs during the onset and decay of the instability, the time-varying behavior can be interpreted based on this representation.

As the equivalence ratio is increased during the ramp up, there is a sudden increase in amplitude at some critical value, which represents the onset of the instability. The relatively narrow distribution of the standard deviation indicates the repeatability of this behavior. Similarly, during the down ramp, the amplitude is also observed to suddenly decrease rapidly, corresponding to the decay of the instability. The difference in equivalence ratio between curves showing this sudden increase and decrease describes the level of hysteresis of the transition.

As the ramp time is reduced, the area separating the onset and decay curves decreases, as indicated in the Stable to Strong Azimuthal Instabilities section. There is also a slight difference in amplitude during onset and decay, which occurs generally in the range of $\phi = 0.85$ – 0.95 where the amplitude tends to be higher during the downward ramp. The response of the harmonic components is qualitatively similar, but the difference in amplitude

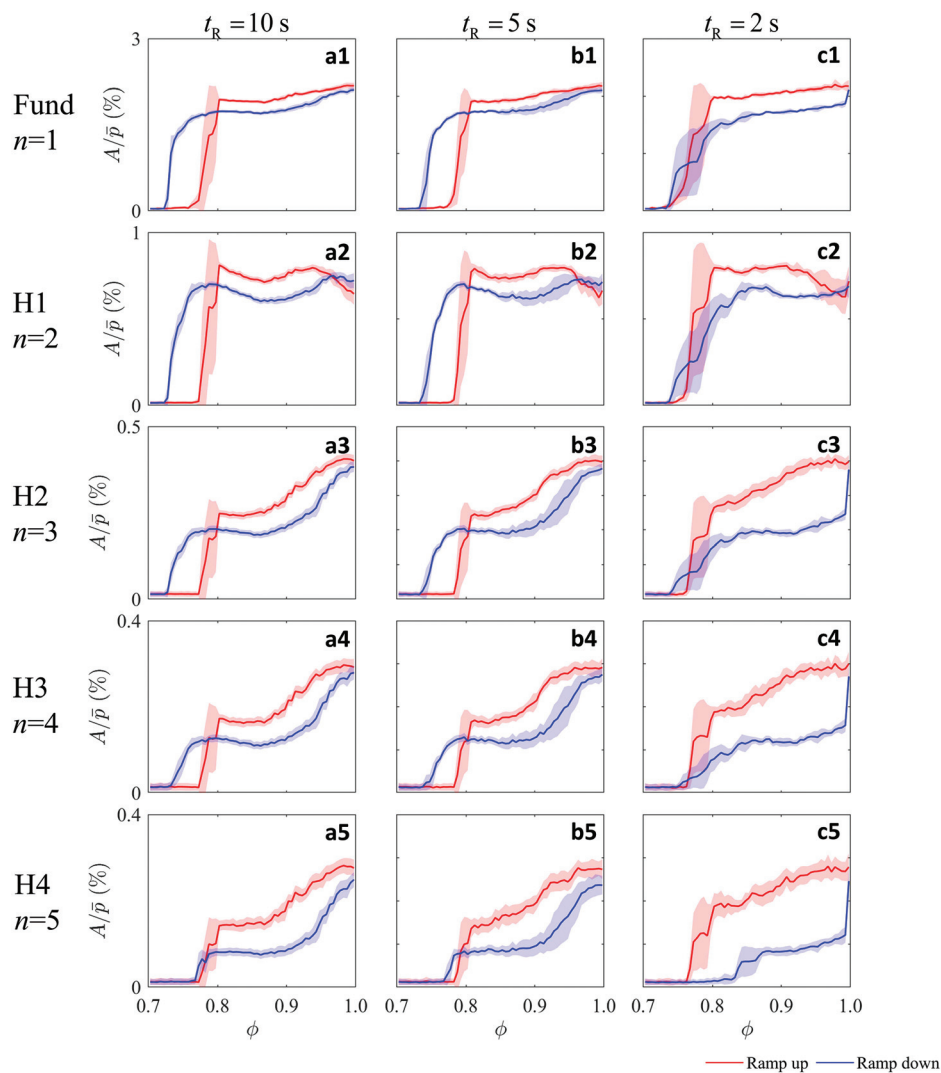


Fig. 5 Mean and standard deviation of the amplitude and equivalence ratio (shaded region) during up/downward ramp for (a) $t_r = 10$ s, (b) $t_r = 5$ s, and (c) $t_r = 2$ s. From top to bottom: (1) fundamental mode, (2) first, (3) second, (4) third, and (5) fourth harmonic components.

during the upward and downward ramps increases with the order of the harmonic. The hysteresis behavior for the harmonic components is similar to the fundamental component, with reducing hysteresis for increased ramping rates. However, a notable exception is the fourth harmonic ($n = 5$), which shows notably less hysteresis behavior for the longer ramping rate experiments.

It is also instructive to examine the hysteresis of the nature angle during the upward and downward ramps, which is shown in Fig. 6. Again, average behavior across multiple runs is evaluated to make more general observations. Focusing first on the fundamental component of the mode shown in the top row, a clear set of modal preferences are established during instability onset. As the equivalence ratio increases during ramp up, the nature angle shifts initially to a predominantly counterclockwise spinning mode ($\chi > 0$ deg), before switching to a strong clockwise spinning mode ($\chi \approx -42$ deg). As the ramping time is decreased, the peak nature angle and the rate of change of the mode switch also tend to increase (see, for example, Fig. 6(c1)). Similarly, this behavior can also be clearly observed in the second harmonic behavior (Fig. 6(c2)). However, for both higher harmonics during upward ramps, and for the fundamental and all harmonics during downward ramps, such behavior is not observed. It is also notable that in this representation, the overshoot behavior of the nature angle is not clearly observed in the fundamental component. This is likely due to the

variability in the start time of the instability growth during multiple repeat measurements. This indicates that there is not a specific equivalence ratio which gives rise to the extreme nature angle, but rather that this is a transient feature, which is based on the modal trajectory during the onset of high-amplitude instability.

Similar observations regarding the amount of hysteresis can be made using this nature angle plot, with the hysteresis in general reducing with increasing ramp rate, and negligible hysteresis present for the fourth harmonic ($n = 5$) component. However, if hysteresis is present both in the amplitude and mode of oscillation, it is useful to examine these simultaneously.

The combined dependence of the mode amplitude and nature angle is shown in Fig. 7 during both upward and downward ramps at different rates, for fundamental and harmonic components. A binning width for χ of 0.4 deg was used to construct these plots. During the onset of the upward ramp, there is a sharp change in nature angle for the fundamental mode which appears to precede the large change in amplitude. After the onset, the amplitude is always large, and the fundamental component is always strongly spinning. The route during the downward ramp is similar, but shows some modest differences at intermediate amplitudes, where mixed modes preferentially occur. Plotted in this manner, the amount of hysteresis appears to be significantly reduced, which indicates that the amplitude and nature angle are very closely

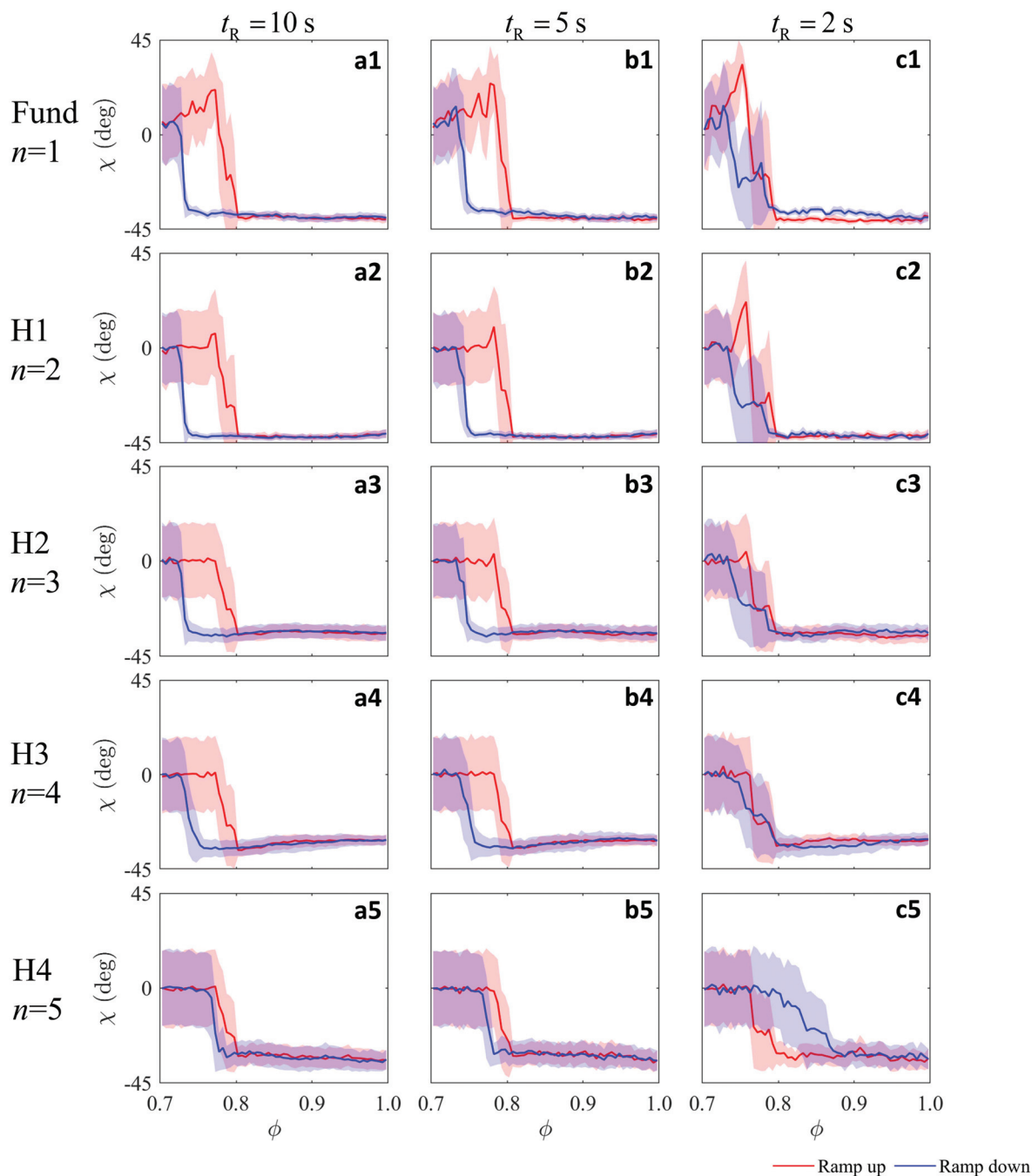


Fig. 6 Mean and standard deviation of the nature angle and equivalence ratio (shaded region) during up/downward ramp for (a) $t_R = 10$ s, (b) $t_R = 5$ s, and (c) $t_R = 2$ s. From top to bottom: (1) fundamental mode, (2) first, (3) second, (4) third, and (5) fourth harmonic components.

coupled, and while both illustrate hysteresis behavior, these behaviors are not separate.

Additionally, similar behavior is observed for the majority of the harmonic components. However, the third harmonic ($n=4$) component shows slightly different behavior, where the peak instability amplitudes are associated with mixed modes. For this component, the highest nature angles are not associated with the highest instability amplitudes. This behavior can also be observed in the nature angle time series in Figs. 2 and 3.

Finally, the relationship between the relative amplitudes of the harmonic components and the fundamental component is investigated in Fig. 8. The average amplitudes are calculated and plotted over scatter plots of amplitude in order to indicate the variability

of the amplitude ratios. A bin size of 0.1 in terms of the x -axis is used for the averaging. Each harmonic is coded by color, and the scale of the x -axis is raised to the power of the mode order n in order to demonstrate the approximately linear scaling of these, which implies a quadratic dependence of the higher harmonics on the fundamental component. Similar scaling relationships have been reported previously in longitudinal modes in single sectors [43] and azimuthal modes in annular configurations [28]. However, in the current plot, the curves are a function of the time-varying amplitude during the upward and downward ramps. Here, the upward and downward ramp curves collapse, demonstrating that the amplitudes of the harmonics remain a function of the fundamental component amplitude.

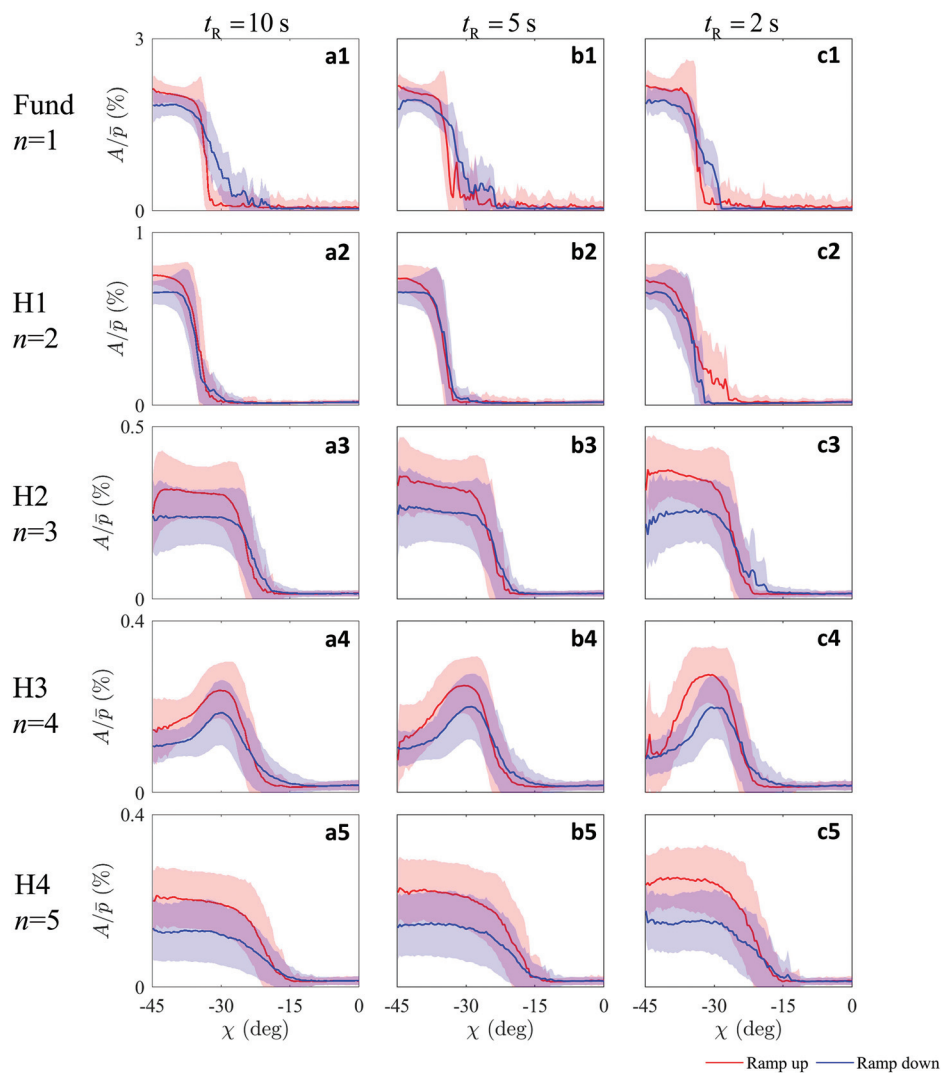


Fig. 7 Mean amplitude and standard deviation (shaded region) plotted against nature angle during up/downward ramp for (a) $t_R = 10$ s, (b) $t_R = 5$ s, and (c) $t_R = 2$ s. From top to bottom: (1) fundamental mode, (2) first, (3) second, (4) third, and (5) fourth harmonic components.

Plotting in this manner also allows the previously observed behavior of the first harmonic on Fig. 2 to be examined in more detail. It was previously described that after the onset of the high-amplitude instability, the amplitude of the first harmonic decreases, as the other components increase and attain their maximum values. The orange curves in Fig. 8 show this clearly with the nonmonotonic behavior at large amplitudes of the fundamental mode. The first harmonic amplitude increases quadratically with the fundamental amplitude until $(A_1/\bar{p} \times 100)^2 = 4$, before decreasing sharply beyond this amplitude. It should be noted that while the amplitude of these components varies as a function of the axial pressure measurement location along the inlet duct, this nonmonotonic behavior of the first harmonic remains similar irrespective of measurement location. While plotting in this manner makes this relationship explicit, further investigation of the relationship of the harmonics may be required to explain this behavior.

Conclusions

In this paper, we present an experimental investigation of dynamic operation in a lab-scale annular combustor under choked operating conditions. The equivalence ratio is ramped linearly in both upward and downward directions in order to identify the

transient acoustic responses of azimuthal instabilities. Operating the facility under pressurized conditions ensures well-defined acoustic boundary conditions and enables the generation of very high-amplitude instabilities with significant harmonic content. Time series analysis reveals the existence of a distinct, repeatable, preferential modal pathway during the onset of high-amplitude self-excited instabilities. During amplitude growth, a strong CCW mode is generated initially, before a rapid switch to a strong CW mode which persists during the high-amplitude oscillations. Increasing the ramping rate increases the nature angle of this precursor state. In addition, the nature angle exhibits a repeatable local minima before the final spinning mode state stabilizes, reaching instantaneously an almost pure spinning state.

Hysteresis behavior is examined and observed in both the amplitude and nature angle of the instability, which depends on the time history of the combustor state, and in general decreases with increasing ramping rate. The generation of very high-amplitude instabilities also permits the effect of hysteresis on the harmonic components of the mode to be investigated. While these are shown to largely follow the fundamental mode, some notable differences are observed, including the nonlinear response of the amplitude of the first harmonic component, the preference for mixed modes of the third harmonic component, and the lack of hysteresis in the fourth harmonic.

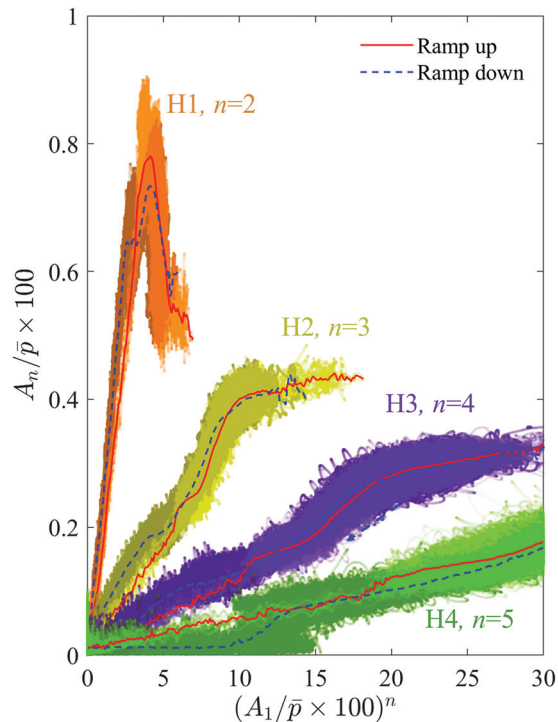


Fig. 8 Dependence of amplitude of harmonic components upon amplitude of fundamental mode. This figure includes all repeat cases. Color denotes the order of n of the harmonic component. Data points of upward/downward ramps are illustrated as lighter/darker color. To identify the general behavior, the parameters are averaged over three repeat cases with a bin size of 0.1 in terms of the x-axis. The solid/dashed lines show the average behavior of upward/downward direction of ramps.

Characterizing these features in a pressurized annular combustor for the first time permits the investigation of novel physical phenomena associated with the transient dynamics of azimuthal instabilities in annular chambers. Furthermore, it also provides unique insights into important precursors to the onset of such instabilities, which may aid the development of future control and mitigation strategies. Finally, these results may be of significant interest to the simulation community, in order to identify the physics of mode onset in practically relevant system.

Acknowledgment

We also acknowledge CBOne for the design and manufacture of the IPA facility.

Funding Data

- European Union's Horizon 2020 research and innovation program (Grant Agreement Nos. 677931 (TAIAC) and 765998 (ANNULIGHt); Funder ID: 10.13039/100010661).

References

- [1] Schuermans, B., Bellucci, V., and Paschereit, C. O., 2003, "Thermoacoustic Modeling and Control of Multi Burner Combustion Systems," *ASME Paper No. GT2003-38688*.
- [2] Lieuwen, T. C., and Yang, V., 2005, *Combustion Instabilities in Gas Turbine Engines: Operational Experience, Fundamental Mechanisms, and Modeling*, American Institute of Aeronautics and Astronautics, Reston, VA.
- [3] Gellert, B., 2013, *Modern Gas Turbine Systems*, Woodhead Publishing, Sawston, UK.
- [4] Krebs, W., Flohr, P., Prade, B., and Hoffmann, S., 2002, "Thermoacoustic Stability Chart for High-Intensity Gas Turbine Combustion Systems," *Combust. Sci. Technol.*, **174**(7), pp. 99–128.
- [5] Seume, J. R., Vortmeyer, N., Krause, W., Hermann, J., Hantschk, C.-C., Zangl, P., Gleis, S., Vortmeyer, D., and Orthmann, A., 1998, "Application of Active Combustion Instability Control to a Heavy Duty Gas Turbine," *ASME J. Eng. Gas Turbines Power*, **120**(4), pp. 721–726.
- [6] Noiray, N., and Schuermans, B., 2013, "On the Dynamic Nature of Azimuthal Thermoacoustic Modes in Annular Gas Turbine Combustion Chambers," *Proc. R. Soc. A: Math., Phys. Eng. Sci.*, **469**(2151), p. 20120535.
- [7] Noiray, N., Bothien, M., and Schuermans, B., 2010, "Analytical and Numerical Analysis of Staging Concepts in Annular Gas Turbines," *n³—International Summer School and Workshop on Non-Normal and Non Linear Effects in Aero and Thermoacoustics*, Munich, Germany, May 17–20.
- [8] Wolf, P., Staffelbach, G., Gicquel, L. Y., Müller, J. D., and Poinso, T., 2012, "Acoustic and Large Eddy Simulation Studies of Azimuthal Modes in Annular Combustion Chambers," *Combust. Flame*, **159**(11), pp. 3398–3413.
- [9] Worth, N. A., and Dawson, J. R., 2012, "Cinematographic OH-PLIF Measurements of Two Interacting Turbulent Premixed Flames With and Without Acoustic Forcing," *Combust. Flame*, **159**(3), pp. 1109–1126.
- [10] Worth, N. A., and Dawson, J. R., 2013, "Modal Dynamics of Self-Excited Azimuthal Instabilities in an Annular Combustion Chamber," *Combust. Flame*, **160**(11), pp. 2476–2489.
- [11] Worth, N. A., and Dawson, J. R., 2013, "Self-Excited Circumferential Instabilities in a Model Annular Gas Turbine Combustor: Global Flame Dynamics," *Proc. Combust. Inst.*, **34**(2), pp. 3127–3134.
- [12] Bourgoignie, J.-F., Durox, D., Moeck, J. P., Schuller, T., and Candel, S., 2013, "Self-Sustained Instabilities in an Annular Combustor Coupled by Azimuthal and Longitudinal Acoustic Modes," *ASME Paper No. GT2013-95010*.
- [13] Berenbrink, P., and Hoffmann, S., 2000, "Suppression of Dynamic Combustion Instabilities by Passive and Active Means," *ASME Paper No. 2000-GT-0079*.
- [14] Bauerheim, M., Salas, P., Nicoud, F., and Poinso, T., 2014, "Symmetry Breaking of Azimuthal Thermo-Acoustic Modes in Annular Cavities: A Theoretical Study," *J. Fluid Mech.*, **760**, pp. 431–465.
- [15] Ghirardo, G., Juniper, M. P., and Moeck, J. P., 2015, "Stability Criteria for Standing and Spinning Waves in Annular Combustors," *ASME Paper No. GT2015-43127*.
- [16] Dawson, J. R., and Worth, N. A., 2015, "The Effect of Baffles on Self-Excited Azimuthal Modes in an Annular Combustor," *Proc. Combust. Inst.*, **35**(3), pp. 3283–3290.
- [17] Morgans, A. S., and Stow, S. R., 2007, "Model-Based Control of Combustion Instabilities in Annular Combustors," *Combust. Flame*, **150**(4), pp. 380–399.
- [18] Noiray, N., Bothien, M., and Schuermans, B., 2011, "Investigation of Azimuthal Staging Concepts in Annular Gas Turbines," *Combust. Theory Modell.*, **15**(5), pp. 585–606.
- [19] Faure-Beaulieu, A., Indlekofer, T., Dawson, J. R., and Noiray, N., 2020, "Experiments and Low-Order Modelling of Intermittent Transitions Between Clockwise and Anticlockwise Spinning Thermoacoustic Modes in Annular Combustors," *Proc. Combust. Inst.*, **38**(4), pp. 5943–5951.
- [20] Bourgoignie, J. F., Durox, D., Moeck, J. P., Schuller, T., and Candel, S., 2015, "Characterization and Modeling of a Spinning Thermoacoustic Instability in an Annular Combustor Equipped With Multiple Matrix Injectors," *ASME J. Eng. Gas Turbines Power*, **137**(2), p. 021503.
- [21] Ghirardo, G., and Gant, F., 2019, "Background Noise Pushes Azimuthal Instabilities Away From Spinning States," e-print [arXiv:1904.00213v1](https://arxiv.org/abs/1904.00213v1), pp. 1–4.
- [22] Dawson, J. R., and Worth, N. A., 2014, "Flame Dynamics and Unsteady Heat Release Rate of Self-Excited Azimuthal Modes in an Annular Combustor," *Combust. Flame*, **161**(10), pp. 2565–2578.
- [23] Vignat, G., Durox, D., Renaud, A., and Candel, S., 2020, "High Amplitude Combustion Instabilities in an Annular Combustor Inducing Pressure Field Deformation and Flame Blow Off," *ASME J. Eng. Gas Turbines Power*, **142**(1), p. 011016.
- [24] Zettervall, N., Worth, N., Mazur, M., Dawson, J., and Fureby, C., 2019, "Large Eddy Simulation of CH₄-Air and C₂H₄-Air Combustion in a Model Annular Gas Turbine Combustor," *Proc. Combust. Inst.*, **37**(4), pp. 5223–5231.
- [25] Fanaca, D., Alemela, P. R., Ettner, F., Hirsch, C., Sattelmayer, T., and Schuermans, B., 2008, "Determination and Comparison of the Dynamic Characteristics of a Perfectly Premixed Flame in Both Single and Annular Combustion Chambers," *ASME Paper No. GT2008-50781*.
- [26] Fanaca, D., Alemela, P. R., Hirsch, C., and Sattelmayer, T., 2010, "Comparison of the Flow Field of a Swirl Stabilized Premixed Burner in an Annular and a Single Burner Combustion Chamber," *ASME J. Eng. Gas Turbines Power*, **132**(7), p. 071502.
- [27] Mazur, M., Kwah, Y. H., Indlekofer, T., Dawson, J. R., and Worth, N. A., 2020, "Self-Excited Longitudinal and Azimuthal Modes in a Pressurized Annular Combustor," *Proc. Combust. Inst.*, **38**(4), pp. 5997–6004.
- [28] Indlekofer, T., Ahn, B., Kwah, Y. H., Wiseman, S., Mazur, M., Dawson, J. R., and Worth, N. A., 2021, "The Effect of Hydrogen Addition on the Amplitude and Harmonic Response of Azimuthal Instabilities in a Pressurized Annular Combustor," *Combust. Flame*, **228**, pp. 375–387.
- [29] Knoop, P., Culick, F., and Zukoski, E., 1997, "Extension of the Stability of Motions in a Combustion Chamber by Nonlinear Active Control Based on Hysteresis," *Combust. Sci. Technol.*, **123**(1–6), pp. 363–376.
- [30] Lieuwen, T. C., 2002, "Experimental Investigation of Limit-Cycle Oscillations in an Unstable Gas Turbine Combustor," *J. Propul. Power*, **18**(1), pp. 61–67.
- [31] Bonciolini, G., Ebi, D., Doll, U., Weilenmann, M., and Noiray, N., 2019, "Effect of Wall Thermal Inertia Upon Transient Thermoacoustic Dynamics of a Swirl-Stabilized Flame," *Proc. Combust. Inst.*, **37**(4), pp. 5351–5358.

- [32] Culler, W., Chen, X., Samarasinghe, J., Peluso, S., Santavicca, D., and O'Connor, J., 2018, "The Effect of Variable Fuel Staging Transients on Self-Excited Instabilities in a Multiple-Nozzle Combustor," *Combust. Flame*, **194**, pp. 472–484.
- [33] Bonciolini, G., and Noiray, N., 2019, "Bifurcation Dodge: Avoidance of a Thermoacoustic Instability Under Transient Operation," *Nonlinear Dyn.*, **96**(1), pp. 703–716.
- [34] Manikandan, S., and Sujith, R. I., 2020, "Rate Dependent Transition to Thermoacoustic Instability Via Intermittency in a Turbulent Afterburner," *Exp. Therm. Fluid Sci.*, **114**, p. 110046.
- [35] Prieur, K., Durox, D., Schuller, T., and Candel, S., 2017, "A Hysteresis Phenomenon Leading to Spinning or Standing Azimuthal Instabilities in an Annular Combustor," *Combust. Flame*, **175**, pp. 283–291.
- [36] Indlekofer, T., Faure-Beaulieu, A., Noiray, N., and Dawson, J., 2021, "The Effect of Dynamic Operating Conditions on the Thermoacoustic Response of Hydrogen Rich Flames in an Annular Combustor," *Combust. Flame*, **223**, pp. 284–294.
- [37] Ghirardo, G., and Juniper, M. P., 2013, "Azimuthal Instabilities in Annular Combustors: Standing and Spinning Modes," *Proc. R. Soc. A: Math., Phys. Eng. Sci.*, **469**(2157), p. 20130232.
- [38] Humbert, S. C., Moeck, J., Orchini, A., and Paschereit, C. O., 2020, "Effect of an Azimuthal Mean Flow on the Structure and Stability of Thermoacoustic Modes in an Annular Combustor Model With Electroacoustic Feedback," *ASME J. Eng. Gas Turbines Power*, **143**(6), p. 061026.
- [39] Nygård, H. T., Mazur, M., Dawson, J. R., and Worth, N. A., 2019, "Flame Dynamics of Azimuthal Forced Spinning and Standing Modes in an Annular Combustor," *Proc. Combust. Inst.*, **37**(4), pp. 5113–5120.
- [40] Nygård, H. T., Ghirardo, G., and Worth, N. A., 2021, "Azimuthal Flame Describing Functions and Symmetry Breaking in an Azimuthally Forced Annular Combustor," *Combust. Flame*, **233**, p. 111565.
- [41] Ghirardo, G., Nygård, H. T., Cuquel, A., and Worth, N. A., 2020, "Symmetry Breaking Modelling for Azimuthal Combustion Dynamics," *Proc. Combust. Inst.*, **38**(4), pp. 5953–5962.
- [42] Worth, N. A., and Dawson, J. R., 2017, "Effect of Equivalence Ratio on the Modal Dynamics of Azimuthal Combustion Instabilities," *Proc. Combust. Inst.*, **36**(3), pp. 3743–3751.
- [43] Kim, K. T., 2017, "Nonlinear Interactions Between the Fundamental and Higher Harmonics of Self-Excited Combustion Instabilities," *Combust. Sci. Technol.*, **189**(7), pp. 1091–1106.